Perturbation Stability of Frictional Sliding With Varying Normal Force*

P. E. Dupont
Assoc. Mem. ASME.

D. Bapna

Aerospace and Mechanical Engineering,
Boston University,
Boston MA 02215

In many systems, the normal force at friction contacts is not constant, but is instead a function of the system's state variables. Examples include machine tools, friction dampers, brake systems and robotic contact with the environment. Friction at these contacts has been shown to possess dynamics associated with changes in normal force. In an earlier paper, the authors derived a critical value of system stiffness for stability based on a linearized analysis of constant velocity sliding (Dupont and Bapna, 1994). In this paper, the domain of attraction for the steady sliding equilibrium point is characterized for a system in which normal force is coupled to tangential displacement. Perturbations consisting of sudden changes in the displacement and velocity of the loading point are considered. These perturbations can be viewed as either actuator disturbances or changes in control input. The effect and interaction of the frictional and geometric parameters are elucidated. The results are applicable to the design and analysis of systems in which steady motion without friction-induced limit cycles is desired.

1 Introduction

Most mechanical systems include friction interfaces and are of finite stiffness. As a result, the potential for unsteady motion in machines is widespread. Since this type of motion is usually detrimental to system performance, a large body of literature has developed which is devoted to techniques for the design and analysis of systems with friction (Armstrong-Hélouvry et al., 1994; Ibrahim, 1994). All techniques involve approximations of the actual system and perhaps the most important approximation in this case is the choice of friction model.

A majority of the literature on frictional instabilities employs friction models in which normal force is constant (Armstrong-Hélouvry et al., 1994). In many important applications, however, there exists a coupling between normal force at a friction interface and other forces or displacements in the system. In analyzing systems of this type, it is critical to include not only this coupling, but also any friction dynamics induced by the coupling.

Those papers that do treat varying normal force have typically assumed that the frictional dependence is linear (Ibrahim, 1994). This is not surprising since the relevance of friction dynamics has only recently been recognized and experimentally-tested dynamic friction models have not been widely available (Armstrong-Hélouvry, 1993; Dupont and Dunlap, 1995).

An exception is the work of Oden and his colleagues who study dry friction between elastic bodies subject to a power law normal response (Oden and Martins, 1985). Normal vibrations of the slider produce an apparent coefficient of friction which typically differs from the velocity-independent interface coefficient of friction. The application of this model to the stability analysis of a pin-on-disk apparatus appears in Tworzydlo et al. (1994).

Using a rigid-body approach, several authors have addressed the existence and modeling of frictional dynamics associated with varying normal force (Hobbs and Brady, 1985; Lockner et al., 1986; Linker and Dieterich, 1992). In two other papers, (Dieterich and Linker, 1992; Dupont and Bapna, 1994), linearized stability criteria have been developed for steady sliding motion of systems subject to the dynamic friction law proposed in Linker and Dieterich (1992). Since the friction law is nonlinear, however, the linearized stability criteria apply for small perturbations of unknown magnitude.

In this paper, we address the question of how the geometry and the load-dependent friction properties of a system affect its ability to reject disturbances and track commanded inputs. We do so for one important geometry in which normal force is coupled by system stiffness to displacement at the friction interface. We employ the friction model of Linker and Dieterich (1992) which is applicable for the low velocities and small displacements of boundary lubrication. While friction can differ between systems, the qualitative trends of this model could provide insights regarding the behavior of other friction models. A Coulomb-like instantaneous response to changes in normal force is a limiting case of this model.

The paper is arranged as follows. In the next section, the friction model is defined and its response to changes in normal force and velocity are described. In Section 3, the system geometry under consideration is presented and its governing equations are derived. In Section 4, the stability of perturbations to steady sliding is studied in the phase plane. The domains of attraction are considered for step changes in load-point displacement and velocity. The effects of frictional and geometric parameters on transient response are summarized. The case of zero load-point velocity is also considered. The paper concludes with a summary of design guidelines for systems of this type.

2 Friction Model

It is often observed experimentally that friction cannot be represented by an algebraic equation relating system state variables (e.g., sliding velocity) to friction force. Rather, the friction force itself possesses dynamics (Armstrong-Hélouvry et al., 1994). During stick slip, this is usually manifested as a higher friction coefficient during the acceleration phase of the slip than during the deceleration phase.

In lubricated contacts at velocities sufficient to eliminate solid to solid contact, it is most likely the fluid film dynamics which control the evolution of friction force (Hess and Soom, 1990; Harnoy et al., 1994). At low velocities under boundary lubrica-

* This work was supported in part by the National Science Foundation under grant MSS-9302190.

Contributed by the Technical Committee on Vibration and Sound for publication in the JOURNAL OF VIBRATION AND ACOUSTICS. Manuscript received Jan. 1995. Associate Technical Editor: R. Ibrahim.

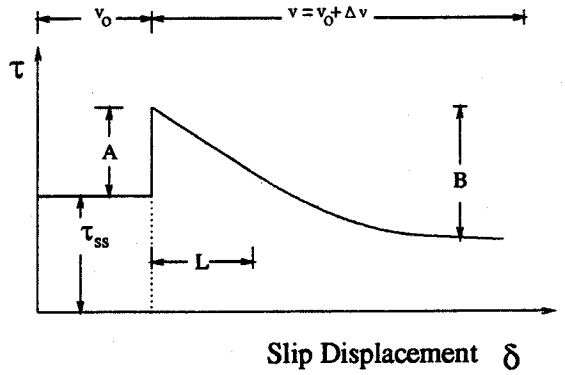

Fig. 1 Response of average friction shear stress τ to step change in velocity, Δv

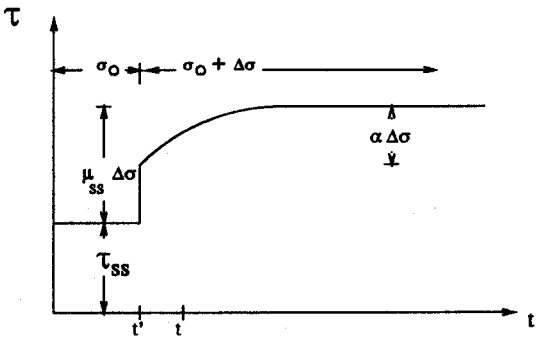

Fig. 2 Response of average friction shear stress τ to step change in normal stress, $\Delta\sigma$

tion, it is likely that the evolution of the asperity contacts determines the friction dynamics (Dieterich, 1979; Dieterich and Linker, 1992).

In boundary lubrication, the response to a step change in velocity has been studied experimentally for a variety of materials including steel on steel, teflon on steel, glass, plastic, wood and rock (Dieterich, 1991; Dupont and Dunlap, 1995). The friction force for a step increase in velocity evolves as shown in Fig. 1. Depending on the materials and lubricant, there may be an instantaneous viscous effect of magnitude A. This is followed by an exponential decay of magnitude B to the final steady-state friction level associated with $v_0 + \Delta v$. (In the model which follows, the changes in friction stress denoted by A and B correspond to the velocity step, $\Delta v = (e - 1)v_0$ where $e = 2.71828 \ldots$.) For those materials tested, this decay appears to occur over characteristic sliding distances (Dieterich, 1991; Dupont and Dunlap, 1995).

Several researchers have studied the transient behavior of friction in response to changes in normal force (Hobbs and Brady, 1985; Lockner et al., 1986; Linker and Dieterich, 1992). All observed that a sudden increase (decrease) in normal force causes a sudden increase (decrease) in friction and an evolutionary increase (decrease) in friction to a new steady-state level as sliding proceeds. The response for a step increase in normal stress is depicted in Fig. 2. The evolutionary component of the response is given by $\alpha\Delta\sigma$ while the instantaneous component is $(\mu_{ss} - \alpha)\Delta\sigma$.

Linker and Dieterich (1992) proposed the following model which has been used in several papers to study the stability of systems with varying normal force (Dieterich and Linker, 1992; Dupont and Bapna, 1994).

$$\tau = \sigma\left[\mu_* + A \ln\left(\frac{v}{v_*}\right) + B\theta\right] \tag{1}$$

$$\dot{\theta} = -\frac{v}{L}\left[\ln\left(\frac{v}{v_*}\right) + \theta\right] - \frac{\alpha}{B\sigma}\dot{\sigma} \tag{2}$$

To be consistent with the notation of earlier papers, the friction law is written in terms of normal stress, σ, and friction shear stress, τ. The reader should understand that these are average quantities which refer to the normal and friction forces divided by apparent area of contact.

In this equation, θ is a frictional state variable while A, B and α are as shown in Figs. 1 and 2. μ_* is the steady-state coefficient of friction at the reference velocity, v_*. L is the characteristic sliding distance controlling the evolutionary response to changes in both velocity and normal stress. This model is used in the remainder of the paper.

For the case of constant normal stress, Dieterich (1979) provides a physical interpretation of the state variable. He proposes that θ is proportional to the apparent age of the asperity junctions. When normal stress can vary, Linker and Dieterich (1992) propose that θ is related to the fraction of the contact area associated with time-dependent creep.

3 Inclined-Spring System

An important case of coupling between normal force and a system's state variables occurs when the friction forces are borne by an elastic member whose normal and tangential displacements are dependent. Consider a block of unit base area, pulled by a spring of stiffness k at an angle ψ as shown in Fig.

Nomenclature

A = parameter expressing dependence of friction on current velocity
B = parameter expressing dependence of friction on prior values of velocity and average normal stress
g = dimensionless average friction shear stress
k = spring constant
k_{cr} = critical spring constant
L = characteristic sliding distance
M_g = maximum overshoot in g
M_ϕ = maximum overshoot in ϕ
P_ϕ = instantaneous change in ϕ due to a load-point displacement perturbation
t = time
v = block velocity
v_0 = load-point velocity
(v_*, μ_*) = reference values of velocity and steady-state friction coefficient
$x, \dot{x}$ = perturbations from steady-state displacement and velocity
x_0 = displacement of load point
α = evolutionary component of steady-state friction coefficient
δ = displacement of block
μ = friction coefficient
μ_{ss} = steady-state friction coefficient
ϕ = natural logarithm of dimensionless velocity
ψ = spring angle
σ = average normal (bearing) stress
σ_0 = nominal normal stress
σ_{ss} = steady-state normal stress
τ = average friction shear stress
θ = friction state variable

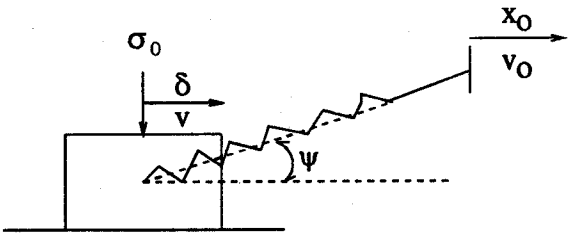

Fig. 3 Inclined-spring model

3. The free end of the spring is pulled at velocity $v_0 = \dot{x}_0$ while the block slides at velocity $v = \dot{\delta}$. When the spring is relaxed, the normal force is given by σ_0. To be consistent with previous literature, the free end of the spring will be called the load point. In an actuated system, the load-point velocity $v_0 = \dot{x}_0$ can be viewed as the control input. In other applications (e.g., brakes), it may be appropriate, through kinematic inversion, to view the load point as held stationary by a constraint force while the surface under the block is in motion. While the inclined-spring system is a simple, idealized model, its geometry is representative of many machine elements.

The normal stress, σ, is given by

$$\sigma = \sigma_0 + k \tan \psi(\delta - x_0) \tag{3}$$

where δ and x_0 are the displacement of the block and load point, respectively. Let

$$\delta = x_{ss} + x$$

so that x represents the shortening of the spring from its steady-state length.

At steady-state

$$\sigma_{ss} = \sigma_0 + k \tan \psi(x_{ss} - x_0) \tag{4}$$

From (3) and (4), normal stress can be written as

$$\sigma = \sigma_{ss} + kx \tan \psi \tag{5}$$

As shown in Dupont and Bapna (1994), quasistatic analysis was found to be a good approximation to the inertial system for a wide range of masses, particularly for the case of $\tan \psi < 0$.

In the equations which follow, τ_{ss}, σ_{ss}, and μ_{ss} represent the steady-state values of friction stress, normal stress and friction coefficient for a load-point velocity of v_0.

For the quasistatic case (i.e., when $m\ddot{\delta}$ is small relative to the other terms),

$$\tau = -k(\delta - x_0) \tag{6}$$

We introduce dimensionless coordinates for velocity and shear stress given by

$$\phi = \ln\left(\frac{v}{v_0}\right) \tag{7}$$

and

$$g = \frac{\tau - \tau_{ss}}{\sigma_{ss}}, \tag{8}$$

respectively. Combining Eqs. (1), (2), (3) and (6), the quasistatic motion of the system is described by

$$\dot{g} = \frac{kv_0}{\sigma_{ss}}(1 - e^{\phi})$$

$$\dot{\phi} = \frac{kv_0(1 - e^{\phi})}{A\sigma_{ss}(1 - \tan \psi g)}\left[\frac{1 + \tan \psi\mu_{ss}}{1 - \tan \psi g} - \tan \psi\alpha\right]$$

$$+ \frac{v_0 e^{\phi}}{AL}\left[\frac{(1 + \tan \psi\mu_{ss})g}{1 - \tan \psi g} + (B - A)\phi\right] \tag{9}$$

Dividing the second equation by the first yields

$$\frac{d\phi}{dg} = \frac{1}{A(1 - \tan \psi g)}\left[\frac{1 + \tan \psi\mu_{ss}}{1 - \tan \psi g} - \tan \psi\alpha\right]$$

$$+ \frac{\sigma_{ss}}{kAL}\left(\frac{e^{\phi}}{1 - e^{\phi}}\right)\left[\frac{(1 + \tan \psi\mu_{ss})g}{1 - \tan \psi g} + (B - A)\phi\right] \tag{10}$$

Equation (10) describes phase plane trajectories for the quasistatic motion of the inclined-spring system with the state variable law given by (1, 2) and the normal stress given by (3).

Trajectories were obtained numerically using a fourth-order, variable-step-size, Runge-Kutta method. The trajectories were generated by switching between (9) and (10). Equation (10) was used for $\phi > 0.3$ while (9) was used otherwise. This switching was required due to the limitations of the integration routine.

3.1 Stationary Load Point, $v_0 = 0$. Consider the special case when the system is initially in motion and the load point is suddenly brought to rest. It is possible to obtain an analytic solution for this case given by

$$\frac{d\phi}{dg} = \frac{1}{A(1 - \tan \psi g)}\left[\frac{1 + \tan \psi\mu_*}{1 - \tan \psi g} - \tan \psi\alpha\right]$$

$$+ \frac{\sigma_*}{AkL}\left[\frac{(1 + \tan \psi\mu_*)g}{1 - \tan \psi g} + (B - A)\phi\right]. \tag{11}$$

This equation is written in terms of μ_* and σ_* to emphasize that the initial and steady-state velocities are different.

Defining

$$\gamma = \left(\frac{B - A}{A}\right)\frac{\sigma_*}{kL},$$

Equation (11) then reduces to

$$\frac{d\phi}{dg} + \gamma\phi = \frac{1 + \tan \psi\mu_*}{A(1 - \tan \psi g)^2} - \frac{\tan \psi\alpha}{A(1 - \tan \psi g)}$$

$$- \frac{\sigma_*(1 + \tan \psi\mu_*)}{AkL}\left(\frac{g}{1 - \tan \psi g}\right). \tag{12}$$

By substituting $\tan \psi = \alpha = 0$ in (12), the differential equation describing the case of constant normal stress can be obtained. The result is equivalent to that of Gu et al. (1984).

Solving (12) for the general case, we find

$$\phi = ce^{-\gamma g} + \frac{1 + \tan \psi\mu_*}{A \tan \psi}\left(\frac{1}{1 - \tan \psi g} + \frac{A}{B - A}\right)$$

$$+ \frac{e^{-\gamma[g - (1/\tan\psi)]}}{A}\left\{\frac{1 + \tan \psi\mu_*}{\tan \psi^2}\left(\gamma + \frac{\sigma_*}{kL}\right) + \alpha\right\}$$

$$\times \left[\ln(1 - \tan \psi g) + \sum_{n=1}^{\infty} \frac{\left\{\frac{-\gamma}{\tan \psi}(1 - \tan \psi g)\right\}^n}{n \times n!}\right] \tag{13}$$

The convergence of the series in (13) follows from the ratio test.

A necessary condition for contact between the block and surface is that the term $(1 - \tan \psi g)$, in the equation above, be positive. This follows because we can express σ as

$$\sigma = \sigma_*(1 - \tan \psi g) \tag{14}$$

In the context of the inclined-spring model, this means that the block may leave the surface if the spring is stretched too much when it is pulling the block out of the surface or if it is compressed too much while pulling the block into the surface.

For both a moving and stationary load point, the following values from Linker and Dieterich (1992) were used to generate the trajectories depicted in the remainder of the paper.

$$A = 0.0145, \quad B = 0.0160, \quad L = 10^{-6}\ \text{m}$$

$$\sigma_0 = 5 \times 10^6\ \text{N/m}^2, \quad \mu_{ss} = 0.7, \quad \alpha = 0.56$$

4 Perturbations

Previously, two necessary conditions for steady sliding at constant velocity were derived (Dieterich and Linker, 1992; Dupont and Bapna, 1994). The first is that the spring angle, ψ, should lie outside the steady-state friction cone defined by μ_{ss} or

$$1 + \mu_{ss} \tan \psi > 0. \tag{15}$$

The second, obtained through linearization, indicates the minimum spring stiffness, k_{cr}, necessary for steady sliding. It is given by

$$k_{cr} = \frac{\sigma_{ss}(B - A)}{L\{1 + (\mu_{ss} - \alpha) \tan \psi\}} \tag{16}$$

A stiffness equal to k_{cr} produces a limit cycle about the steady sliding equilibrium point. The critical stiffness applies to perturbations from equilibrium of sufficiently small size.

In response to a finite perturbation for $k > k_{cr}$, the system may converge back to steady sliding or it may diverge such that the block sticks or attains a high velocity. This could lead to stick slip. Even if the system does converge to the equilibrium point, it may do so in an undesirable manner.

In this section, we investigate the maximum size of stable perturbations (their domain of attraction) and ascertain the dependence of their transient response on the values of spring stiffness k, steady-state friction coefficient μ_{ss}, frictional lag α, and spring angle ψ. It is assumed that perturbations arise either from disturbance forces which drive the system away from the equilibrium point or from sudden changes in commanded input. An example of the latter would be a step change in commanded velocity requiring the system to move to a new equilibrium point. This could correspond to a desired velocity step or to the staircase output of a digital-to-analog converter.

For the quasistatic inclined-spring system, the phase plane, discussed in the next section, is two dimensional. Any perturbation from the equilibrium point of steady sliding can be decomposed into a combination of steps in the displacement and the velocity of the load point (Gu et al., 1984). The jump to a zero load-point velocity is treated as a separate case. A stationary load point could represent an intentional dwell time or a stiction interval of the actuator.

4.1 Phase Plane. It is convenient to represent the evolution of the system with time on a plane defined by the axes $(\phi, g) = (\ln (v/v_0), ((\tau - \tau_{ss})/\sigma_{ss}))$. In this plane, each point represents a unique combination of velocity and shear strength and has a value of state variable given by (1). The origin represents the steady sliding condition for load-point velocity, v_0. In the phase plane, constant-state curves are straight lines with slope A. The line $\theta = 0$ passes through the origin.

At steady state, $\dot{\theta} = \dot{\sigma} = 0$. From (2), $\theta_{ss} = -\ln (v/v_0)$. Substitution of this value into (1) yields the following equation

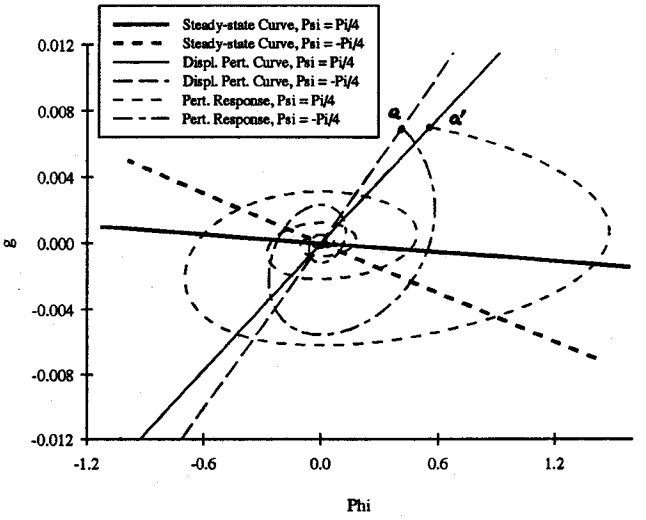

Fig. 4 Characteristic curves for inclined-spring model with $\psi = -\pi/4$ and $\psi = \pi/4$. Trajectories for load-point displacement perturbations are shown for the two spring angles.

for the locus of points corresponding to steady sliding for all values of load-point velocity.

$$\phi = \left(\frac{1 + \tan \psi \mu_{ss}}{A - B}\right) \frac{g}{1 - \tan \psi g} \tag{17}$$

The steady-state curves for $\psi = \pm\pi/4$ are shown in Fig. 4. For constant normal stress, these curves reduce to a line through the origin with slope, $(A - B)$.

One type of perturbation corresponds to a sudden change in the velocity of the load point. Assuming that the system was initially at steady state, this type of perturbation instantaneously moves the equilibrium point to a new position on the steady-state curve. The trajectory taken to the new equilibrium point is described by (9).

A second type of perturbation involves a change in shear stress without any change in load-point velocity. This can be caused by a sudden change in load-point displacement. To picture such a perturbation in the phase plane, consider that the evolution Eq. (2) for θ can be expressed as:

$$d\theta = -\frac{d\delta}{L}\left[\ln\left(\frac{v}{v_0}\right) + \theta\right] - \frac{\alpha}{B\sigma} d\sigma \tag{18}$$

When the load point is suddenly displaced, the block does not move instantaneously and hence $d\delta = 0$. In this case, the equation above simplifies to

$$d\theta = -\frac{\alpha}{B\sigma} d\sigma \tag{19}$$

with

$$d\sigma = -\tan \psi d\tau$$

The shear stress, τ, as given by (1), when expressed in terms of the dimensionless velocity, ϕ becomes

$$\tau = \sigma[\mu_{ss} + A\phi + B\theta]$$

Differentiation and substitution of expressions for $d\sigma$, $d\theta$ and σ yields the following differential equation for the load-point displacement perturbation curve.

$$\frac{d\phi}{d\tau} = \frac{1}{A}\left[\frac{1 - \alpha \tan \psi}{\sigma_0 - \tan \psi \tau} + \frac{\tan \psi \tau}{(\sigma_0 - \tan \psi \tau)^2}\right] \tag{20}$$

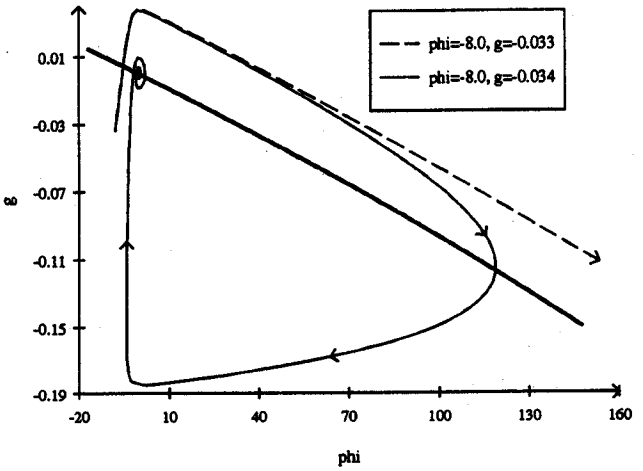

Fig. 5 Trajectory stability for $\psi = \pi/4$, $k = 3k_{cr}$. The stability boundary lies between the stable and unstable trajectories shown.

If the system is at (ϕ_1, g_1) when the perturbation occurs, the equation can be integrated to obtain

$$P_\phi = \phi - \phi_1 = \frac{1}{A}\left[\alpha \ln\left(\frac{1 - \tan\psi g}{1 - \tan\psi g_1}\right) + \frac{(1 + \tan\psi\mu_{ss})(g - g_1)}{(1 - \tan\psi g_1)(1 - \tan\psi g)}\right] \quad (21)$$

Figure 4 depicts the load-point displacement perturbation curves for two spring angles, $\psi = \pm\pi/4$. For constant normal stress, these curves reduce to a line of constant state, θ, which lies approximately midway between the pair of curves shown.

The figure also illustrates, for each spring angle and initial conditions $(\phi_i, g_i) = (0, 0)$, load-point displacement perturbations and the subsequent response of the system. The perturbation moves the system instantaneously from the origin to point $a(a')$ for $\psi = -\pi/4$ ($\psi = \pi/4$). The ensuing trajectory back to the origin follows a solution to (9). During the perturbation, the increase in ϕ, denoted P_ϕ, for $\psi = \pi/4$ is slightly larger than that of $\psi = -\pi/4$. During the ensuing motion, however, the maximum block velocity for $\psi = \pi/4$ is 2.4 times that for $\psi = -\pi/4$.

As can be seen from this figure, any general perturbation from the origin (initial condition in the phase plane) can be decomposed into perturbations in load-point displacement and velocity. In addition, certain load point trajectories may be modeled as a sequence of perturbations.

4.2 Domain of Attraction. The linearized stability result indicates that the origin of the phase plane is stable for spring stiffnesses greater than k_{cr} under sufficiently small perturbations. Given a value of k, the domain of attraction is the set of points in the phase plane for which the nonlinear system converges to the origin (is asymptotically stable).

4.2.1 Moving Load Point. Figure 5 depicts one stable and one unstable trajectory for $\psi = \pi/4$. While no equation for the boundary of the domain of attraction is known, this boundary exists and lies between the stable and unstable trajectories shown in the figure.

Note that stable trajectories near the stability boundary experience very high velocities before reaching equilibrium. To give an illustration, for the stable trajectory shown in Fig. 5, ϕ goes as high as 125. The velocity at this point is $e^{125}v_0$ ($= 1.93558 \times 10^{54}v_0$). This is well outside the range of ϕ for which the model is valid. Thus, knowledge of the location of the actual boundary is not necessary.

A more appropriate stability boundary can be defined by prescribing bounds on either shear stress transients or velocity transients or both. Shear stress transients could be important if an actuator is operating near saturation. In precision motion control applications, velocity transients would be of considerable concern.

Suppose, for example, that one is interested in determining the maximum step increase in load-point velocity for which the maximum velocity overshoot of the block does not exceed $\phi = 7$ ($v_{max}/v_{final} = e^7$). Since the system is time invariant, phase plane trajectories do not cross each other. The maximum velocity step can be obtained by starting at the point given by $\phi = 7$, $\partial g/\partial\phi = \infty$ and following the system backwards in time until the steady-state curve is reached. Figure 6 shows the maximum velocity step perturbation $\Delta\phi$ as a function of spring stiffness for five spring angles.

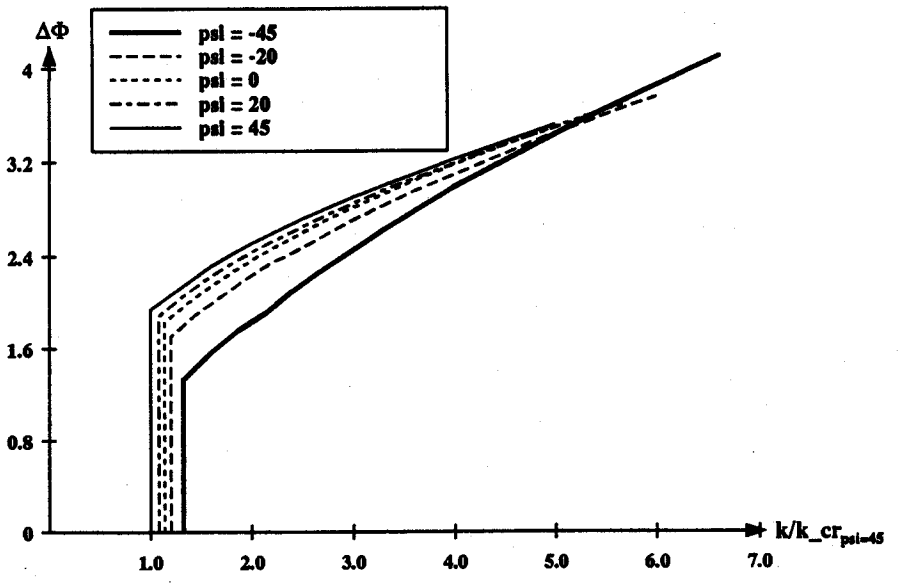

Fig. 6 Maximum load-point velocity step perturbation $\Delta\phi$ as a function of k/k_{cr} ($\psi = \pi/4$) for various spring angles (expressed in degrees). Based on maximum velocity overshoot of $\phi = 7$.

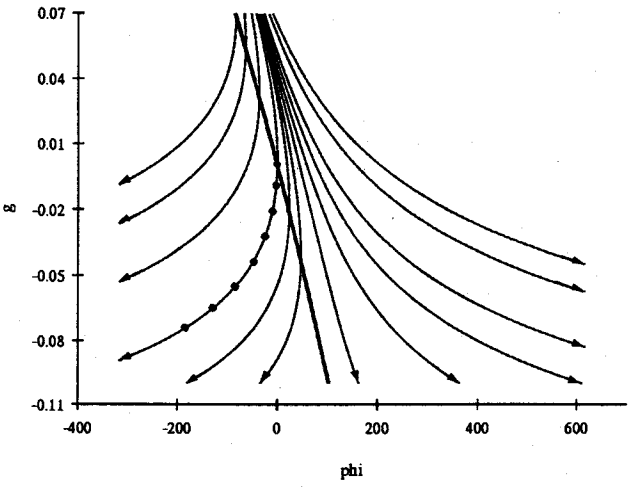

Fig. 7 Stationary load point with $\psi = \pi/4$ and $k = 3k_{cr}$. The dotted trajectory is followed by the sliding block when the load-point, originally moving with velocity v_0, stops suddenly. Similar trajectories are obtained for other spring angles.

4.2.2 Stationary Load Point. Before proceeding to the analysis, we need to note that for the case of a stationary load point, the usual interpretation of k_{cr} is not possible. In this case, the equilibrium is at $\phi = -\infty$ and linearization about $-\infty$ is inappropriate for a nonlinear system. Nonetheless, the value of k does determine the domain of attraction and the rate at which the system converges to the equilibrium point.

For constant normal stress, the stability boundary for trajectories described by a simplified (12) is given by a line which, for $k > 0$, intersects the ϕ-axis at a positive value of ϕ (Gu et al., 1984). Velocities along trajectories starting to the right of this line tend toward infinity while those of trajectories to the left of the line tend toward zero (i.e., the block stops). As k increases, this line shifts to the right along the ϕ axis, thus increasing the region in the phase plane where the trajectories are stable.

In the case of variable normal stress, the phase plane trajectories defined by (13) are depicted in Fig. 7 for $\psi = \pi/4$ and various initial conditions. Unlike the constant normal stress case, an equation for the stability boundary is not easily obtained. It can be seen from the figure, however, that there is a boundary separating the stable and unstable trajectories.

As was the case for a moving load point, some trajectories within the domain of attraction, while asymptotically stable, attain high velocities before the system comes to rest. For all practical purposes, these trajectories can be considered unstable. If a maximum allowable velocity is specified, we can find a trajectory such that for all the initial conditions to the left of this trajectory, velocities will always remain less than the maximum allowable velocity. This trajectory will serve as a practical stability boundary.

Setting $(d\phi/dg) = 0$ in (12) we get

$$\phi = \frac{1}{A\gamma(1 - \tan\psi g)}\left\{\frac{1 + \tan\psi\mu_*}{(1 - \tan\psi g)} - \tan\psi\alpha\right\} - \frac{1}{B - A}\left\{\frac{(1 + \tan\psi\mu_*)g}{1 - \tan\psi g}\right\} \quad (22)$$

Once a maximum allowable velocity is chosen, the corresponding g can be calculated from (22) and the trajectory through this point computed. Since the trajectories do not cross each other in the phase plane, this trajectory can be considered the stability boundary.

4.3 Effect of Parameters. Several parameters affect the location of both the actual and transient-limited stability boundaries. These are the stiffness, k, the steady-state coefficient of friction, μ_{ss}, its evolutionary component, α, and the spring angle, ψ. Due to the nonlinearity of the system, it is difficult to describe their effect and interrelationship quantitatively. Through simulation, however, it is possible to evaluate their qualitative effect on transient response for moving and stationary load points. These effects are summarized in Table 1.

The novel aspects of this work involve the geometric parameter, ψ, and the frictional lag parameter, α. The ensuing discussion focuses on their effect on displacement and velocity perturbations of the load point. From Fig. 4, note that load-point displacement perturbations follow curves with a steep slope in the phase plane. Conversely, load-point velocity perturbations follow steady-state curves with small negative slopes.

As shown by the trajectories depicted in Fig. 4, it is the ψ-dependent trajectory shape which determines the relative velocity overshoot in response to load-point displacement perturba-

Table 1 Effect of parameters on transient response. M_ϕ and M_g are the maximum overshoot in block velocity and friction stress, respectively. P_ϕ is the instantaneous change in block velocity due to a displacement perturbation. All perturbations are those of the load point. Note that there is no M_g for $v_0 = 0$. (↑ = increases, ↓ = decreases, * = for k/k_{cr} ($\psi = \pi/4$) < 5.25)

	Effect of Increasing Parameter	
Parameter	$v_0 \neq 0$	$v_0 = 0$
α	$\psi > 0$: $M_\phi \uparrow, M_g \uparrow$ $\psi < 0$: $M_\phi \downarrow, M_g \downarrow$ Displacement Perturbation: $\psi > 0$: $P_\phi \downarrow$; $\psi < 0$: $P_\phi \uparrow$	$\psi > 0$: $M_\phi \uparrow$ $\psi < 0$: $M_\phi \downarrow$
ψ	$k_{cr} \downarrow$ Displacement Perturbation: $P_\phi \uparrow, M_\phi \uparrow$ Velocity Perturbation: $M_\phi \downarrow^*, M_g \downarrow$	(No k_{cr}) $M_\phi \uparrow$
k	$M_\phi \downarrow, M_g \downarrow$	$M_\phi \downarrow$
μ_{ss}	Effect is small for $\mu_{ss} \in [0.56, 0.70]$	Effect is small

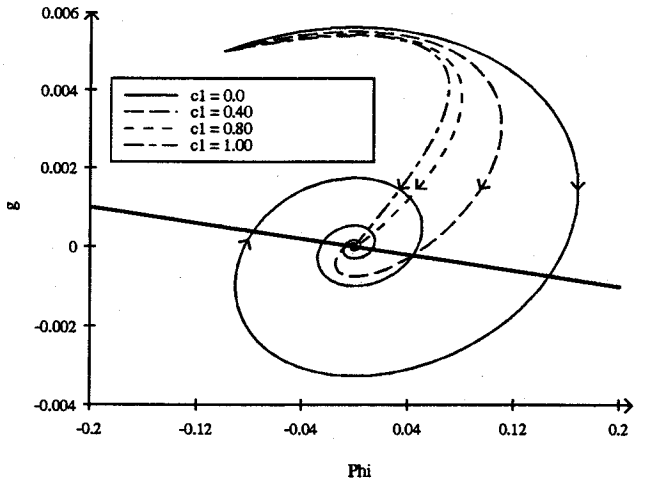

Fig. 8 Effect of α for $\psi = -\pi/4$. $c_1 = \alpha/\mu_{ss}$, $\mu_{ss} = 0.70$ and $k = 3k_{cr}$

tions. Negative spring angles produce smaller maximum velocities. For the same reason, if the maximum velocity overshoot is specified, negative spring angles allow larger load-point displacement perturbations.

The result is not the same, however, if one considers load-point velocity perturbations as shown in Fig. 6 (for fixed velocity overshoot). Although increasing ψ produces a flatter trajectory, the rate of convergence (in the velocity direction) is only weakly dependent on ψ for small $k > k_{cr}$. The larger size of the allowable velocity steps for $\psi > 0$ in Fig. 6 is consequently due primarily to the trend toward a horizontal steady-state curve for increasing ψ. As k increases, however, the relative rate of convergence for negative spring angles increases such that at $k \approx 5.25k_{cr}$ ($\psi = \pi/4$), M_ϕ is independent of ψ.

For all spring angles, the frictional lag parameter α reduces the effect of the spring angle. This is made clear in Fig. 8 which depicts the effect of α on the phase plane trajectories for $\psi = -\pi/4$ given a single set of initial conditions. This observation can be applied directly to load-point velocity perturbations as the steady-state curve (17) is independent of α. During load-point displacement perturbations, however, there is the additional influence of α on P_ϕ in (21).

5 Conclusions

Much effort has been devoted to friction compensation (controller design) based on the assumption that the mechanical and frictional properties of the system are fixed. It is also possible, however, to reconsider mechanical and lubricant design from the viewpoint of producing a system which is easier to control. The analysis of this paper has revealed, for the inclined-spring system, the interrelationship between the geometric property ψ, the stiffness property k, and the frictional property α. It has also been shown that the best choice of these parameters depends on the type of input trajectories or perturbations which are expected.

If one is designing a system which can be modeled by the inclined-spring system, the foremost consideration is to ensure that the stiffness exceeds the critical value necessary for steady sliding. Negative spring angles ($\psi < 0$) require stiffer springs for stability and the spring angle must lie outside the friction cone to avoid jamming. If, however, the system is likely to experience load-point displacement perturbations, (e.g., short periods of rapid load point slip) negative spring angles produce less velocity overshoot.

If load-point velocity perturbations are expected (e.g., velocity step inputs), increasing the spring angle will decrease the velocity overshoot for $k < 5k_{cr}$ ($\pi/4$). It will also decrease the friction stress overshoot and thus decrease the maximum load borne by the load-point actuator.

Frictional lag associated with changes in normal force can have a significant effect on the transient dynamics as shown in Fig. 8. According to the sign of the selected spring angle, the lag can be either stabilizing or destabilizing. To achieve prescribed performance criteria, selection of materials, lubricants, spring stiffness and spring angle should be considered concurrently.

While friction does vary from system to system, its basic components, including frictional memory, are the same. Consequently, the results presented here could provide qualitative insight into the behavior of a variety of systems.

6 References

Armstrong-Hélouvry, B., 1993, "Stick-slip and Control in Low-speed Motion," *IEEE Trans. on Auto. Control,* Vol. 38, No. 10, pp. 1483–1496.

Armstrong-Hélouvry, B., Dupont, P., and Canudas de Wit, C., 1994, "A Survey of Models, Analysis Tools and Compensation Methods for the Control of Machines With Friction," *Automatica,* Vol. 30, No. 7, pp. 1083–1138.

Dieterich, J. H., 1979, "Modeling of Rock Friction: 1. Experimental Results and Constitutive Equations," *Journal of Geophysical Research,* Vol. 84, pp. 2161–2168.

Dieterich, J. H., 1991, "Micro-mechanics of Slip Instabilities with Rate- and State-dependent Friction," *Eos, Trans. Am. Geophys. Union,* Fall Meeting Abstract Volume, p. 324.

Dieterich, J. H., and Linker, M. F., 1992, "Fault Stability under Conditions of Variable Normal Stress," *Geophysical Research Letters,* Vol. 19, No. 16, pp. 1691–1694.

Dupont, P., and Bapna, D., 1994, "Stability of Sliding Frictional Surfaces with Varying Normal Force," ASME JOURNAL OF VIBRATION AND ACOUSTICS, Vol. 116, pp. 237–242.

Dupont, P., and Dunlap, E., 1995, "Friction Modeling and PD Compensation at Very Low Velocities," ASME *Journal of Dynamic Systems, Measurement and Control,* Vol. 117, No. 1, pp. 8–14.

Gu, J. C., Rice, J. R., Ruina, A. L., and Tse, S. T., 1984, "Slip Motion and Stability of a Single Degree of Freedom Elastic System with Rate and State Dependent Friction," *J. Mech. Phy. Solids,* Vol. 32, pp. 167–196.

Harnoy, A., Friedland, B., and Rachoor, H., 1994, "Modeling and Simulation of Elastic and Friction Forces in Lubricated Bearings for Precise Motion Control," *Wear,* Vol. 172, pp. 155–165.

Hess, D. P., and Soom, A., 1990, "Friction at a Lubricated Line Contact Operating at Oscillating Sliding Velocities," *J. of Tribology,* Vol. 112, No. 1, pp. 147–152.

Hobbs, B., and Brady, B., 1985, "Normal Stress Changes and the Constitutive Law for Rock Friction (Abstract)," *Eos trans, AGU,* Vol. 66, p. 382.

Ibrahim, R. A., 1994, "Friction-induced Vibration, Chatter, Squeal and Chaos, Part ii: Dynamics and Modeling," *Applied Mechanics Reviews,* Vol. 47, No. 7, pp. 227–253.

Linker, M., and Dieterich, J., 1992, "Effects of Variable Normal Stress on Rock Friction: Observations and Constitutive Equations," *Journal of Geophysical Research,* Vol. 97,(B4), pp. 4923–4940.

Lockner, D., Summer, R., and Byerlee, J., 1986, "Effects of Temperature and Sliding Rate on Frictional Strength of Granite," *Pure Appl. Geophys.,* Vol. 124, pp. 445–485.

Oden, J., and Martins, J., 1985, "Models and Computational Methods for Dynamic Friction Phenomena," *Comput. Methods Appl. Mech. Eng.,* Vol. 52, Nos. 1–3, pp. 527–634.

Tworzydlo, W., Becker, E., and Oden, J., 1994, "Numerical Modeling of Friction-induced Vibrations and Dynamic Instabilities," *Applied Mechanics Reviews,* Vol. 47, No. 7, pp. 255–274.